Morphology and properties of rigid-rod poly(*p*-phenylene benzobisoxazole) (PBO) and stiff-chain poly(2,5(6)-benzoxazole) (ABPBO) fibres

S. J. Krause, T. B. Haddock and D. L. Vezie
Department of Chemical, Bio and Materials Engineering, Arizona State University, Tempe, AZ 85287, USA

and P. G. Lenhert
Department of Physics, Vanderbilt University, Nashville, TN 37235, USA

and W.-F. Hwang* and G. E. Price
University of Dayton Research Institute, Dayton, OH 45469, USA

and T. E. Helminiak, J. F. O'Brien and W. W. Adams
Materials Laboratory – Polymer Branch, Air Force Wright Aeronautical Laboratories, Wright–Patterson, OH 45433, USA
(Received 3 November 1987; revised 14 January 1988; accepted 14 January 1988)

The morphology of two new high performance polymer fibres, rigid-rod poly(*p*-phenylene benzobisoxazole) (PBO) and stiff-chain poly(2,5(6)-benzoxazole) (ABPBO), has been examined by wide angle X-ray scattering and scanning and transmission electron microscopy. Heat treatment of as-spun PBO and ABPBO fibres produces transversely broadened crystallites, which are unlike uniaxially elongated crystallites in heat treated fibres of rigid-rod poly(*p*-phenylene benzobisthiazole) (PBT) or stiff-chain Kevlar, i.e. poly(*p*-phenylene terephthalamide) (PPTA). Heat treated fibres of PBO have greater three-dimensional crystallinity and long range crystallite ordering than axially disordered PBT, but much less than well ordered PPTA. Fibres of both as-spun and heat treated PBO have a crystalline *c*-axis with high orientation and low paracrystalline disorder, but heat treatment of as-spun fibres of ABPBO significantly increases *c*-axis orientation and decreases *c*-axis paracrystallinity, due to additional extension of the stiff-chain ABPBO molecules. Eventual improvements in orientation and ordering of PBO fibre through improvements in synthesis and processing may, based upon theoretically predicted values, result in up to triple the strength and modulus of commercial PPTA fibre.

(Keywords: tensile modulus; morphology; wide angle X-ray scattering; electron microscopy; poly(*p*-phenylene benzobisoxazole; poly(2,5(6)-benzoxazole))

INTRODUCTION

Recently, there has been a flurry of activity in the development of new high performance polymer fibres with high tensile strength and modulus and excellent thermal and environmental resistance. Du Pont's Kevlar, a stiff-chain poly(*p*-phenylene terephthalamide) (PPTA), was marketed some ten years ago and has emerged as the leading high performance organic polymer fibre for a wide variety of high specific strength applications. Other fibres with improved properties have recently been announced. These include the liquid crystal polyesters (LCP), produced by Celanese, Dartco, and Tennessee Eastman. A drawback to LCPs, however, is modulus lower than PPTA. Another material is Spectra, a gel-spun polyethylene, produced by Allied Chemical. Although it has very high specific strength and modulus, its application potential is limited by its relatively low melting point. Teijin Ltd has also announced plans to market HTM 50, a copolyamide similar to Kevlar, but with improved modulus, strength, and chemical resistance.

Over the past two decades the US Air Force has been developing a new class of aromatic heterocyclic polymers for high performance applications. An earlier material, rigid-rod poly(*p*-phenylene benzobisthiazole) (PBT), was first synthesized by Wolfe *et al.*[1]. PBT has a tensile modulus double that of Kevlar 49 and also significantly improved chemical and thermal resistance. Recently, two new ordered polymers, rigid-rod poly(*p*-phenylene benzobisoxazole) (PBO) and stiff-chain poly(2,5(6)-benzoxazole) (ABPBO), have been synthesized to high molecular weight by Wolfe *et al.*[2]. The chemical structures of these molecules are shown in *Figure 1*. Fibres spun from these materials were also found to have excellent mechanical and thermal properties. In these and other 'ordered polymers' there are direct correlations between the polymer structure and its processability and properties. Indeed, it is the chemical architecture and the ability of these polymers to orient and order that provides

* Present address: Central Research Laboratory, Dow Chemical Company, Midland, MI 48674, USA.

0032-3861/88/081354-11$03.00

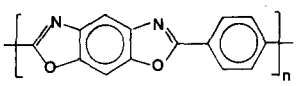

PBO

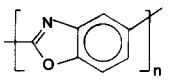

ABPBO

Figure 1 Chemical structure of PBO and ABPBO

the opportunity to achieve unprecedented levels of performance.

The structure and morphology of many high performance polymers have been previously reported, including PPTA[3-10], LCP[11], Spectra[12], and PBT[13-18]. Although the crystal structures of the PBO model compound[18] and polymer[19] and the ABPBO polymer[20] have recently been described, only preliminary work has been reported on the morphology of PBO and ABPBO[21]. The goal of this work was to characterize the morphology of fibres of PBO and ABPBO with wide angle X-ray scattering (WAXS), transmission electron microscopy (TEM) and scanning electron microscopy (SEM). The results are compared to the morphology and mechanical properties of other ordered polymer systems.

BACKGROUND

The morphology of stiff-chain PPTA fibre has been studied by Johnson and co-workers[3-5], Northolt[6,7] and others[8-10] with WAXS, TEM and SEM. In PPTA fibre the molecules are well aligned with the fibre axis and are packed into three-dimensionally (3D) ordered crystallites in which planes of molecules are hydrogen bonded laterally[8]. The crystallites are axially elongated with dimensions up to 40 nm long and 20 nm wide. On a larger scale, regular periodic structures 200 nm to 300 nm in size along the fibre axis have been observed in TEM dark field (DF) images, and a pronounced skin-core structural boundary was observed in SEM fracture studies[10].

Three structural models of PPTA fibre have emerged. In the 'pleated sheet' model[6], molecules are aligned in pleated sheets, which are hydrogen bonded, that extend longitudinally along the fibre axis and project radially from the centre to the circumference of the fibre. In the 'container' model[10], long rod-shaped crystallites about 50 nm in diameter have hydrogen bonded planes aligned radially with respect to the fibre. These are stacked longitudinally and are contained within an external annular skin of continuously staggered molecules. In the 'periodically disordered lattice' model[8] a large fraction of extended chains of PPTA bridge periodically disordered regions between crystalline regions along the length of the fibres.

The morphology of the rigid-rod PBT ordered polymer has been studied extensively by Thomas and co-workers[13-16] and by Odell *et al.*[17]. As-spun PBT fibre contained 2.0 nm crystallites which, upon heat treatment, grew into axially elongated crystallites 10 nm by 20 nm in size. Paracrystalline analysis of selected area electron diffraction (SAED) line broadening of multiple meridional orders gave a low degree of axial disorder of 0.53% and a crystallite axial dimension of 15 nm, which agreed moderately well with TEM imaging studies. Analysis of diffraction results indicated that PBT crystallites, unlike those of 3D ordered PPTA, had only 2D lateral order and lacked the longitudinal registry required for 3D crystallinity. However, TEM bright field (BF) lattice images showed some crystallites with both lateral and longitudinal periodicities, which indicated that at least limited 3D order was present[16], although not to the extent found in the pleated sheets found in PPTA. Samples from a PBT fibre surface showed varying orientation and crystallite size in TEM, while highly oriented and well developed crystallites were observed from the volume of the fibre by WAXS, indicating that, similar to PPTA, a skin-core effect was also present in PBT. No special models for PBT fibre morphology have been proposed, but samples generally showed, upon tension heat treatment, improved alignment of molecules, fibrils, and crystallites and correspondingly improved mechanical properties.

The crystal structure of the PBO model compound[18] and the preliminary structure of the PBO polymer fibre[19] have been published. In the PBO polymer structure, molecules are in a planar conformation in a monoclinic unit cell with lattice parameters of $a = 0.565$ nm, $b = 0.358$ nm and $c = 1.174$ nm, and $\gamma = 102.5°$[15]. The b-axis length is roughly the perpendicular distance between the faces of heterocyclic rings between chains, the a-axis length is roughly the distance between equivalent edges of heterocyclic rings adjacent in the chains, and the c-axis length is the distance along the chain of a single mer unit. The structure and lattice parameters are similar to PBT, except that the PBT a-axis is slightly larger (0.58 nm in the primitive unit cell) than in PBO, possibly due to the non-planarity of the PBT molecules and the larger diameter of the sulphur atoms.

The structure of ABPBO fibre has been reported[20]. It has an orthorhombic unit cell with lengths of $a = 0.606$ nm, $b = 0.338$ nm, and $c = 1.158$ nm[20]. In ABPBO the b-axis and a-axis lengths are also roughly the perpendicular distances between the faces and the edges of heterocyclic rings, respectively, while the c-axis length is the distance along the chain of two repeat units in a planar zig-zag conformation. The structure and lattice parameters are quite similar to ABPBT (poly(2,5-benzothiazole))[20] and ABPBI (poly(2,5-benzimidazole))[22], except that the ABPBI a-axis is somewhat longer (0.72 nm) than that of ABPBO.

The mechanical properties of heat treated fibres of PPTA, PBT, PBO, and ABPBO are listed in *Table 1*. A comparison of specific strength and specific modulus of these fibres and other engineering materials is shown in *Figure 2*.

Table 1 Mechanical properties of some ordered polymer fibres

Material	Strength (GPa)	Modulus (Gpa)	Ductility (% elongation)
PPTA (Kevlar 49)	3.3	132	2.5
(Kevlar 149)	2.7	179	1.5
PBT[14]	3.1	320	1.1
PBO	3.6	370	1.9
ABPBO	3.1	140	2.9

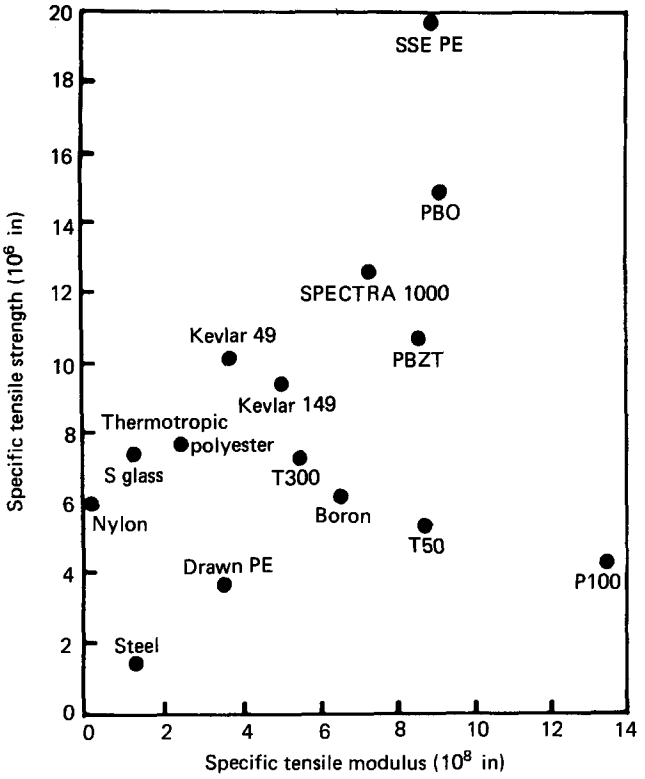

Figure 2 Specific strength and specific modulus of various engineering materials

EXPERIMENTAL MATERIALS AND METHODS

Materials

Fibres were spun by extruding solution through a spinneret die into a water coagulating bath. The fibres were dry jet/wet spun, usually to a high draw ratio, in the air gap between the die and the water bath. The wet fibre was neutralized in NH_4OH overnight and rinsed in distilled water. The fibres were heat treated under tension at elevated temperatures in air.

Wide angle X-ray scattering

WAXS photographs were recorded using flat-film Statton (Warhus) cameras. CuKα radiation was generated by an Elliot GX20 rotating anode X-ray generator with a nickel filter. The sample-to-film distance for the two Statton cameras was 29.2 ± 0.2 mm, as calibrated by the National Bureau of Standards silicon powder, SRM 640.

WAXS diffractometer scans were collected on a Picker FACS-1 automated diffractometer. A copper tube with a graphite crystal incident beam monochromator was used to obtain CuKα X-rays. One millimetre incident beam and diffracted beam collimators were used. The samples were prepared by winding 100 cm of single filament around a cardboard holder to form fibre bundles with diameters from 0.25 mm to 0.7 mm. Hexamethylenetetramine ($C_6H_{12}N_4$) was used as a standard to correct for instrumental line broadening. The hexamine standard was ground to a fine powder and packed into glass capillary tubes to approximate the fibre bundle geometry. After experimenting with these standards, the take-off angle and symmetrically variable aperture were chosen to be 3° and 2 mm for meridional scans and 1° and 0.5 mm for equatorial scans in order to optimize crystallite size measurements. Overlapping reflections from fibre samples were resolved using a curve fit program.

The lateral crystallite sizes were calculated from line breadths of equatorial reflections by using the Debye–Scherrer equation, assuming Gaussian profiles of corrected line breadth. The longitudinal crystallite sizes along the *c*-axis were calculated from line breadths of meridional reflections both by using the Debye–Scherrer equation and by using Hosemann's paracrystallinity analysis[23]. An overall disorder parameter along the *c*-axis was also determined using paracrystallinity analysis. Using the multiple reflections of PBO and ABPBO along the *c*-axis, and assuming they are due to distortions of the second kind, a distortion parameter and average crystallite size can be calculated. Reflections along the meridian were used for crystallite size analysis only if the peak counts were at least five times the background counts. For Gaussian profiles, the following equation can be used:

$$(\partial\beta)^2 = (1/D)^2 + \pi^4 l^4 g^4 / c^2$$

where:

$\partial\beta$ = line breadth of reflection;
D = average crystallite size;
l = index of reflection;
g = disorder parameter;
c = length of *c*-axis.

Plotting $\partial\beta^2$ *versus* l^4 will yield a straight line with a slope of $\pi^4 g^4 / c^4$ and a *y*-intercept of $(1/D)^2$. Both PBO and ABPBO have multiple orders of the (001) reflections. Measuring the half-width and plotting it *versus* l^4 gives the values of g and D. A computer program was used to calculate the half-widths of the reflections. The half-widths were corrected for instrumental line broadening.

Scanning electron microscopy

Internal structure of fibres was examined by fracturing in liquid nitrogen and viewing on an ISI Alpha 9 at magnifications from 100 to 5000. Samples were gold sputter coated to prevent charging and images were recorded on Polaroid type 55 film.

Transmission electron microscopy

TEM images and SAED patterns were taken on a JEOL 100CX at 100 kV and recorded on Kodak 4463 film. Thin samples of fibre were prepared by the detachment replication technique[14]. In short, a sample fibre is placed on the surface of a thin layer of collodion solution, and later, when the solvent has evaporated, the fibre is stripped away leaving a few thin areas detached in the collodion. Subsequently, a 3 mm diameter area of the sample is placed on a copper grid covered with a holey carbon film (0.5–5 μm holes). The collodion is then dissolved away with amyl acetate vapours, leaving the detached fragments to settle onto the holey carbon film on the copper grid.

Coherently diffracting regions of samples were dark field imaged at magnifications from 10 000 to 20 000 with a tilted beam, using the combined first, second, and third equatorial reflections for PBO ($E_1 + E_2 + E_3$), and the combined first and second equatorial reflections for ABPBO ($E_1 + E_2$). Although PBO and ABPBO fibres are significantly more resistant to electron beam damage than are conventional semi-crystalline polymers (e.g.

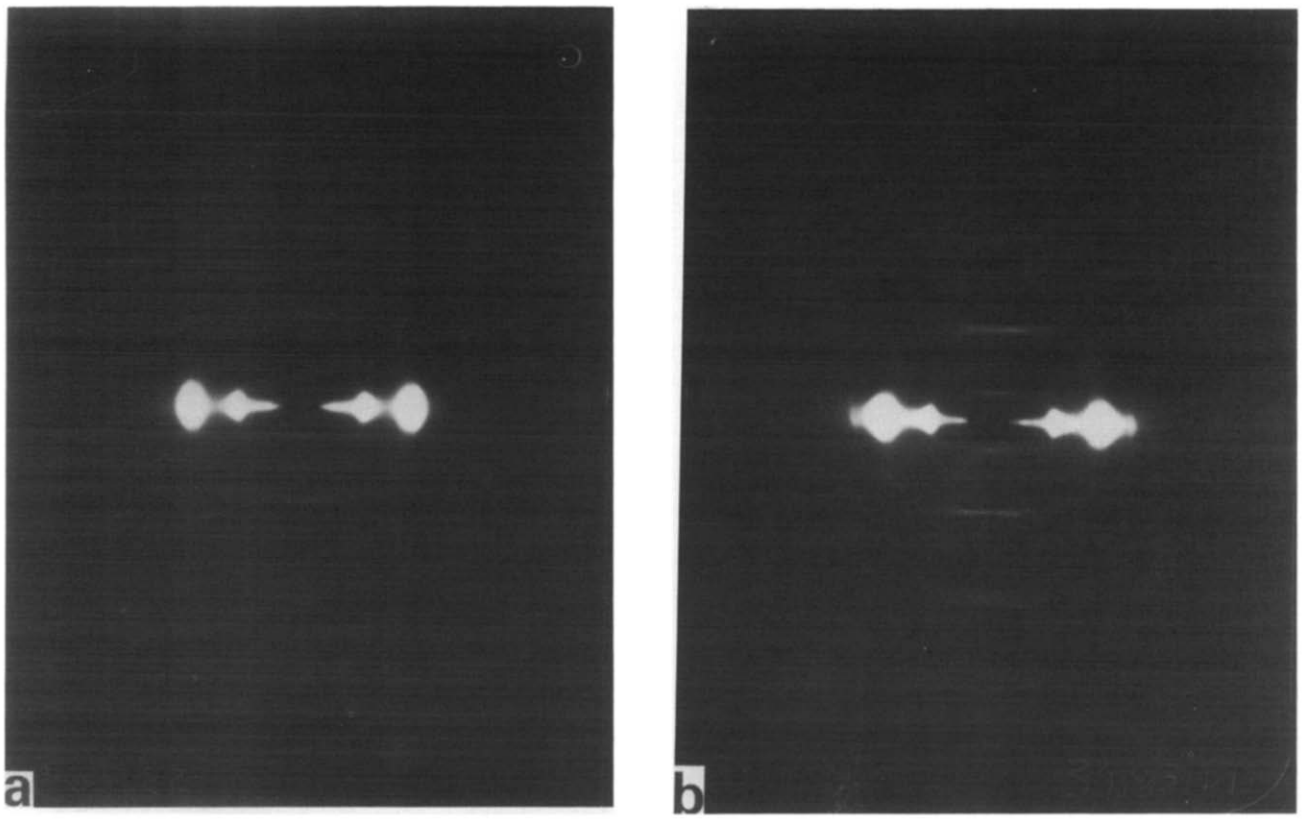

Figure 3 WAXS pattern of PBO fibre in (a) the as-spun and (b) the heat treated condition

polyethylene)[24], loss of diffraction contrast did occur with large electron dosage. To minimize beam damage artefacts, DF images were recorded on fresh areas adjacent to those initially used for focusing.

SAED patterns were taken at a camera length of 76 cm from areas 1–2 μm in diameter. The camera constant was calibrated by measuring d-spacings from gold evaporated onto selected specimens.

RESULTS AND DISCUSSION

Wide angle X-ray scattering

WAXS flat film patterns for as-spun and heat-treated PBO fibre are shown in *Figure 3* and for ABPBO in *Figure 4*. The general features of all patterns are similar. All fibres show strong equatorial reflections which are only slightly arced, indicating that crystallites are highly oriented. Multiple meridional reflections indicate that molecules are also well oriented. The patterns also show a limited number of well defined, off-axis, first order (*hkl*) reflections, indicative of 3D crystallinity of fibres in both the as-spun and the heat treated condition. Significant sharpening of the off-axis (*hkl*) reflections in heat treated fibre for both PBO and ABPBO indicates there is an increase in 3D order and/or crystallite size upon heat treatment.

The 3D crystallinity in PBO contrasts with the axial disorder in PBT where no off-axis (*hkl*) reflections are observed. It may be that, compared to non-planar PBT molecules, the planar molecules of PBO have improved chain axis registry, thus promoting 3D crystallinity in both the as-spun and heat treated fibre. However, only first order (*hkl*) reflections are present in PBO, whereas many higher order (*hkl*) reflections are observed in PPTA, indicating that PBO crystalline structure is not as well ordered as PPTA. The 3D crystallinity observed for ABPBO fibre is not unexpected since it is also observed for fibres of ABPBT and ABPBI[25].

The d-spacings of PBO and ABPBO fibres from flat film patterns are listed in *Table 2* for equatorial reflections and in *Table 3* for meridional reflections. The mean c-axis spacing of PBO and ABPBO from diffractometer data is listed in *Table 4*. For PBO fibre, there are no significant changes in equatorial d-spacings upon heat treatment, indicating that lateral chain packing in crystallites is already well established in the as-spun fibre. Likewise, there is little change in the mean c-axis length of PBO upon heat treatment. This would be expected since PBO is a rigid rod molecule and the c-axis, which is aligned with the chain axis, should be constant.

For ABPBO fibre, the d-spacing of the first equatorial reflection decreases upon heat treatment by about 3%, from 0.623 nm to 0.605 nm. A similar effect was observed for ABPBI fibre, in which the a-axis length was reduced by 11% upon heat treatment[26]. This indicates that for ABPBO, as well as ABPBI, chains become more tightly packed between the edges of the heterocyclic rings in the unit cell. The 0.338 nm d-spacing is reduced by less than 1% upon heat treatment, indicating that the spacing between heterocyclic rings is virtually unchanged. The mean c-axis spacing increases by 1.8% upon tension heat treatment, which means that the chain is more extended. There is also a significant increase in orientation due to both the extension of the chain backbone and alignment of chains during tension heat treatment. An increase in the length of the repeat unit is not unexpected, since ABPBO is not a rigid-rod molecule, but a stiff-chain molecule in which conformational defects (which are not

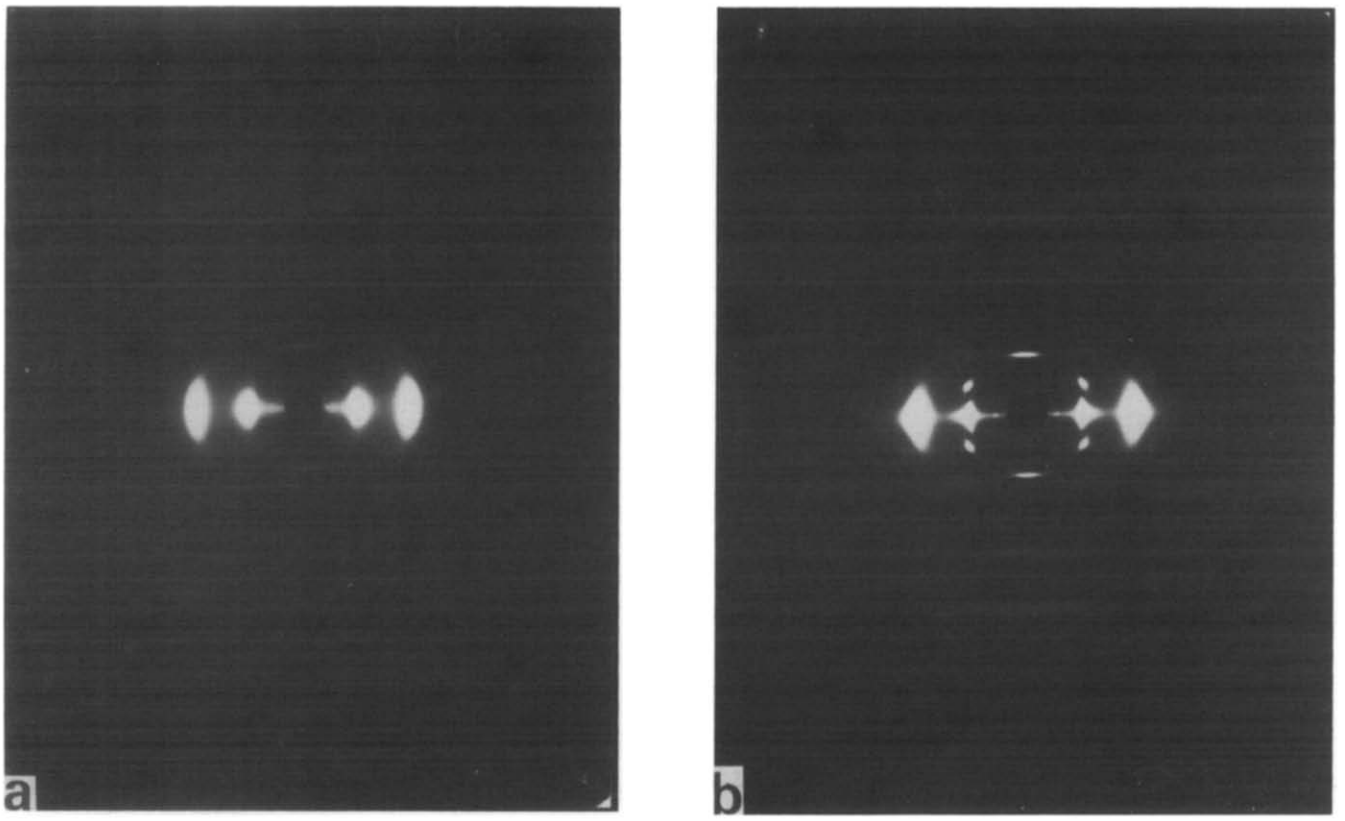

Figure 4 WAXS pattern of ABPBO fibre in (a) the as-spun and (b) the heat treated condition

Table 2 The *d*-spacing, relative intensity, crystallite size, and orientation factor from equatorial reflections of PBO and ABPBO

Sample	*d* (nm)	I_{rel}	*D* (nm)	f_x
PBO – as-spun	0.552	100	9.4	−0.483
	0.349	66	6.1	} overlapping
	0.326	70	8.1	} reflection
	0.278	2	11.3	
PBO – heat treated	0.551	100	16.7	−0.489
	0.350	43	8.5	} overlapping
	0.327	53	8.8	} reflection
	0.276	3	15.3	
ABPBO – as-spun	0.623	54	5.8	−0.442
	0.338	100	5.6	
ABPBO – heat treated	0.605	100	24.3	−0.493
	0.335	70	9.7	

in an extended, planar zig-zag geometry) along the chain backbone could be extended during tension heat treatment.

PBO and ABPBO crystallite sizes (*D*) from the Scherrer analysis are presented in *Table 2* for equatorial reflections and in *Table 3* for meridional reflections. Mean crystallite sizes from meridional reflections with the Scherrer analysis are given in *Table 4*. The mean meridional crystallite size and the disorder parameter from the Hosemann analysis are given in *Table 5*. These parameters are also listed for PBT and PPTA in *Table 5*.

The average dimensions of the crystallites of PBO in as-spun fibre along the *a*, *b* and *c* axes are 9.4, 6.1 and 15.9 nm, respectively. The larger crystallite size along the *a*-axis compared to the *b*-axis may be a manifestation of the crystal structure dimensions where the unit cell *a*-axis is longer than the *b*-axis. The *c*-axis length is the same from both the Scherrer and the Hosemann analysis. This is reasonable since the disorder parameter, *g*, has a relatively low value of 1.22%. The average crystallite dimensions of PBO in heat treated fibre along the *a*, *b* and *c* axes are 16.7, 8.5 and 21.7 nm. The *c*-axis crystallite size is similar in both the Scherrer and the Hosemann analysis, which is reasonable, since the disorder parameter, *g*, has decreased to an even lower value of 1.07%.

The ratios of crystallite size before and after heat treatment are listed in *Table 6*. Crystallite growth tends to be transverse with respect to the fibre axis since the growth ratio is greatest along the *a*-axis and least along the *c*-axis. The *a*-axis growth occurs between the edges of the heterocyclic rings and may be due to a combination of reduced paracrystalline disorder and an increase in crystallite size. It was not possible to separate these factors due to the limited number of lateral reflections present. Growth along the *c*-axis is relatively limited, indicating that there is already a high degree of axial order in the as-spun state. The value of the disorder parameter of 1.07% is slightly more than for PBT (0.53%), and slightly less than for PPTA (1.7%)[7].

The average dimensions of the crystallites of ABPBO in as-spun fibre along the *a*, *b* and *c* axes are 5.8, 5.6 and 8.3 nm, respectively. The *c*-axis length is slightly more from the Scherrer analysis than from the Hosemann analysis. The value of the disorder parameter, *g*, of 2.38% is somewhat higher than for PBO. Once again, this is probably due to the fact that ABPBO is a stiff-chain polymer, which may have conformational defects along the chain, while PBO is a rigid-rod polymer with no conformational freedom along the length of the chain.

Table 3 The *d*-spacing, relative intensity and crystallite size from meridional reflections of PBO and ABPBO

Sample	*d* (nm)	I_{rel}	*l* index	*D* (nm)
PBO – as-spun	1.190	21	11	—
	0.398	27	3	19.1
	0.300	12	4	22.3
	0.240	100	5	19.4
	0.198	26	6	9.9
	0.171	2	7	—
	0.150	4	8	—
	0.133	33	9	14.8
	0.120	35	10	13.7
	0.109	33	11	12.1
PBO – heat treated	1.198	23	1	—
	0.554	2	2	—
	0.400	28	3	25.9
	0.301	18	4	32.4
	0.240	100	5	24.7
	0.199	2	6	—
	0.172	3	7	—
	0.150	1	8	—
	0.134	40	9	18.4
	0.122	46	10	16.6
	0.109	47	11	12.1
ABPBO – as-spun	0.567	100	2	17.2
	0.286	68	4	10.1
	0.222	40	5	3.6
	0.191	86	6	6.3
	0.168	2	7	—
	0.142	4	8	—
	0.125	28	9	4.3
	0.113	10	10	—
ABPBO – heat treated	1.179	3	1	—
	0.579	100	2	34.2
	0.289	39	4	27.4
	0.228	2	5	—
	0.193	31	6	21.4
	0.145	5	7	—
	0.127	3	8	—
	0.115	1	9	—

Table 4 Mean *c*-axis repeat length and mean meridional crystallite size

Sample	Number of reflections	Mean *c*-axis (nm)	*D* (001) (nm)
PBO – as-spun	10	1.196 ± 0.005	15.9
PBO – heat treated	7	1.201 ± 0.002	21.7
ABPBO – as-spun	8	1.138 ± 0.019	8.3
ABPBO – heat treated	3	1.158 ± 0.002	27.7

The average crystallite dimensions of ABPBO in heat treated fibre along the *a*, *b* and *c* axes are 24.3, 9.7 and 27.7 nm. The *c*-axis crystallite size is similar from both the Scherrer and the Hosemann analyses. However, the disorder parameter, *g*, has decreased to a value of 1.35%, due to removal of conformational defects by chain extension during tension heat treatment. The ratios of crystallite sizes before and after heat treatment are listed in *Table 6*. Crystallite size increases fourfold along the *a*-axis and threefold along the *c*-axis. As with PBO, the *a*-axis growth occurs between the edges of the heterocyclic rings and may be due to a combination of reduced disorder and/or an increase in crystallite size. Growth along the *c*-axis is large, indicating that axial order has been significantly increased compared to the as-spun state. This is also related to a significant increase in axial orientation. The value of the disorder parameter is similar to other ordered polymers.

Scanning electron microscopy

SEM images of fracture surfaces of as-spun and heat-treated PBO are shown in *Figure 5* and of ABPBO in

Table 5 Hosemann's paracrystallinity analysis

Sample	*g* (%)	*D* (nm)
PBO – as-spun	1.22	15.9
PBO – heat treated	1.07	19.5
ABPBO – as-spun	2.38	8.1
ABPBO – heat treated	1.35	23.2
PBT – heat treated[25]	0.53	22.8
PPTA[7]	1.7	70.0

Table 6 Crystallite growth

	HT to AS crystallite size ratio		
Sample	*a*-axis	*b*-axis	*c*-axis
PBO	1.9	1.4	1.2
ABPBO	4.2	1.7	2.9

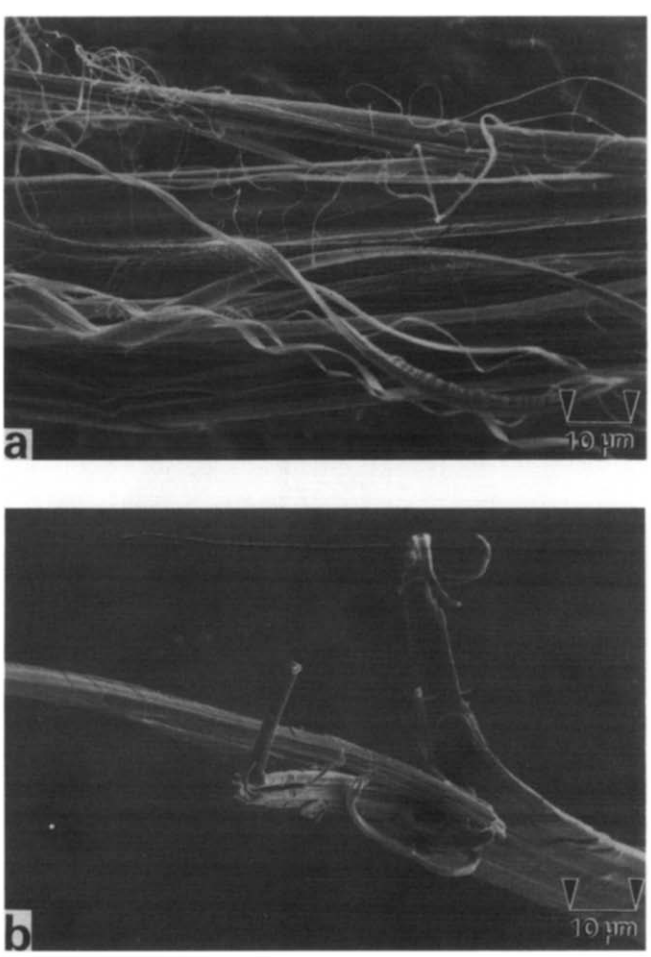

Figure 5 SEM images of fracture surfaces of PBO fibre in (a) the as-spun and (b) the heat treated condition

Figure 6. Both fibres have a similar appearance in the as-spun and heat-treated condition. The images show a fibrillar-type fracture with limited ductility. The structures appear to be of two general types. There are larger fibril bundles which are slightly bent and sometimes twisted, with a diameter of 5–10 μm. The fibrils themselves are finer, 0.2–2 μm in diameter, and are frequently bent, twisted and curled. PBO fibre bundles and fibrils have either a rounded and irregular or a ribbon-like cross section whereas ABPBO bundles and fibrils usually have a rounded and irregular cross section. The fibrils provide connectivity between the larger fibril bundles. On some of the larger fibril bundles, both axial and lateral striations are present. The lateral striations are due to kinking of the fibrils from compressive stresses which are probably induced by recoil during liquid nitrogen fracture. Their appearance is similar to those observed for PBT and PPTA.

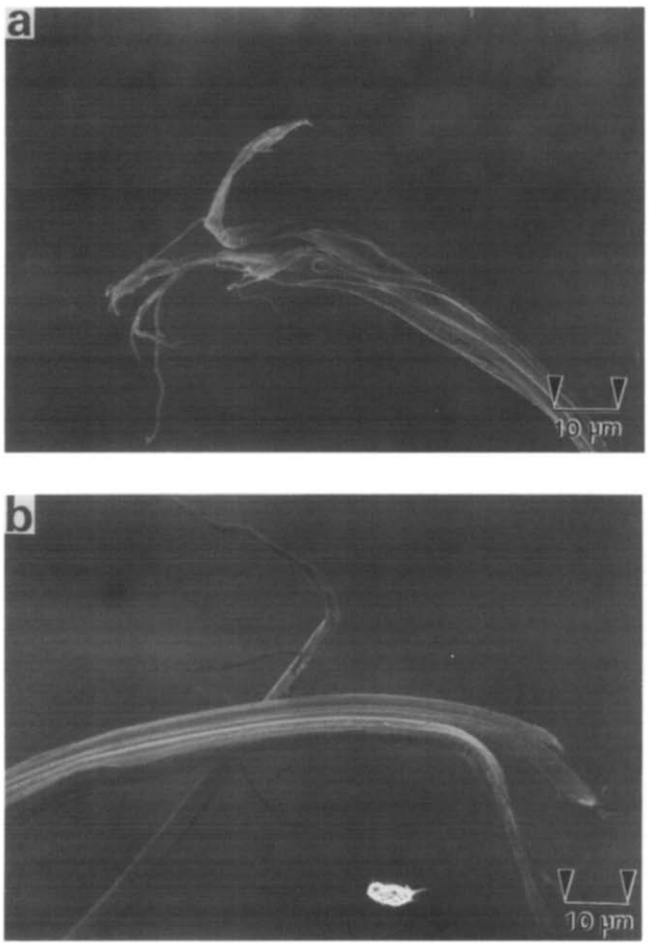

Figure 6 SEM images of fracture surfaces of ABPBO fibre in (a) the as-spun and (b) the heat treated condition

Transmission electron microscopy

Bright field imaging. Low magnification bright field images for as-spun and heat-treated PBO fibre are shown in *Figure 7* and for ABPBO in *Figure 8*. Samples are generally composed of polymer strands which are partially fibrillated into strands or ribbons with widths ranging from about 30 nm up to a few micrometres. A similar ribbon-like fibril geometry is frequently observed for PBO in SEM fracture surface images.

The as-spun samples in *Figures 7a* and *8a* show fewer and slightly thicker fibrils than the heat-treated samples in *Figures 6b* and *7b*. This is due to some loss of ductility during heat treatment. All PBO and ABPBO samples occasionally displayed kinks at the edge or through the cross-section of a strand or fibril. These are induced by compressive mechanical stresses along the fibre axis which occur by bending during detachment replication or by residual stresses generated during processing. In PBO, fibrils have a ribbon-like morphology, similar to PBT. Unlike PPTA, neither PBO nor ABPBO has any 200–500 nm long-range axially periodic structure.

ABPBO samples have a tendency to fibrillate into rounded irregular fibrils in contrast to the ribbon-like fibrils of PBO. The ABPBO fibrils range in size from a few

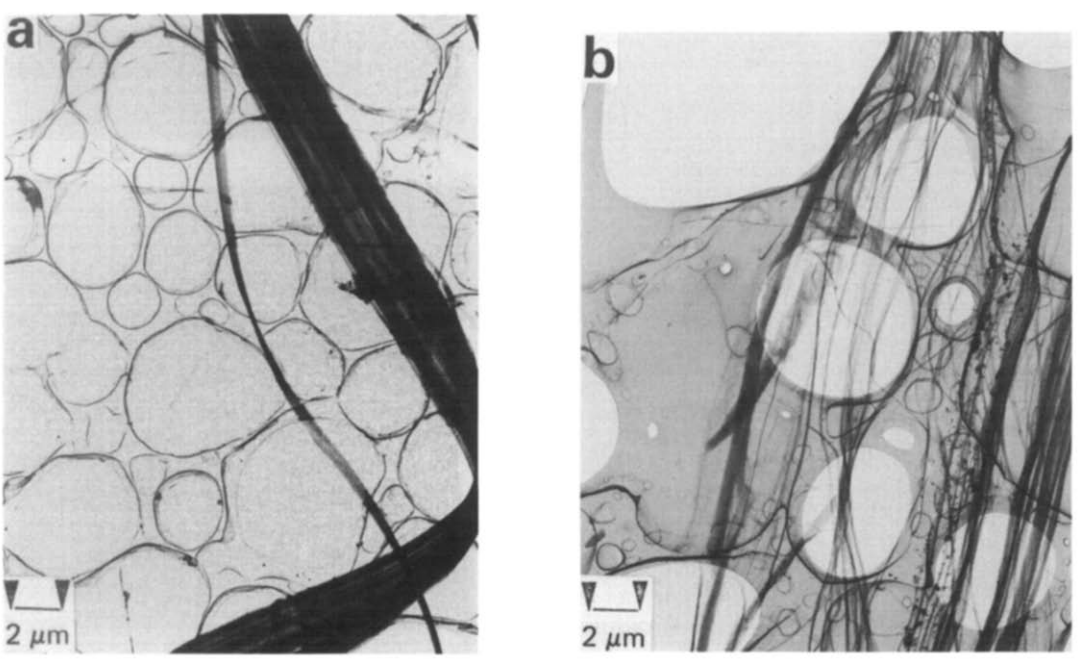

Figure 7 TEM bright field images of PBO fibre in (a) the as-spun and (b) the heat treated condition

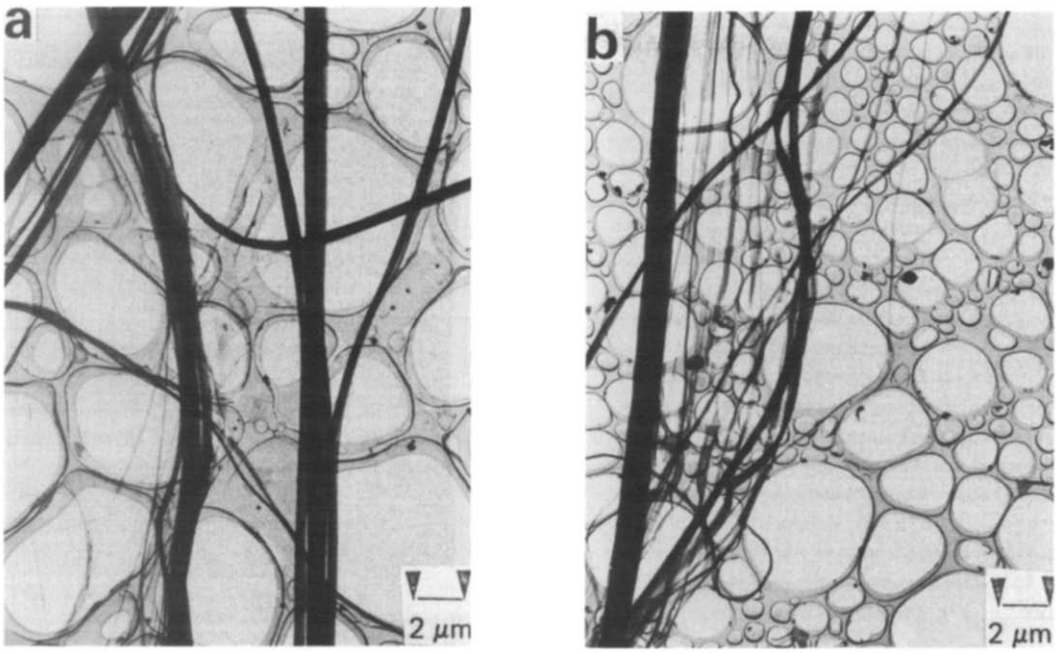

Figure 8 TEM bright field images of ABPBO fibre in (a) the as-spun and (b) the heat treated condition

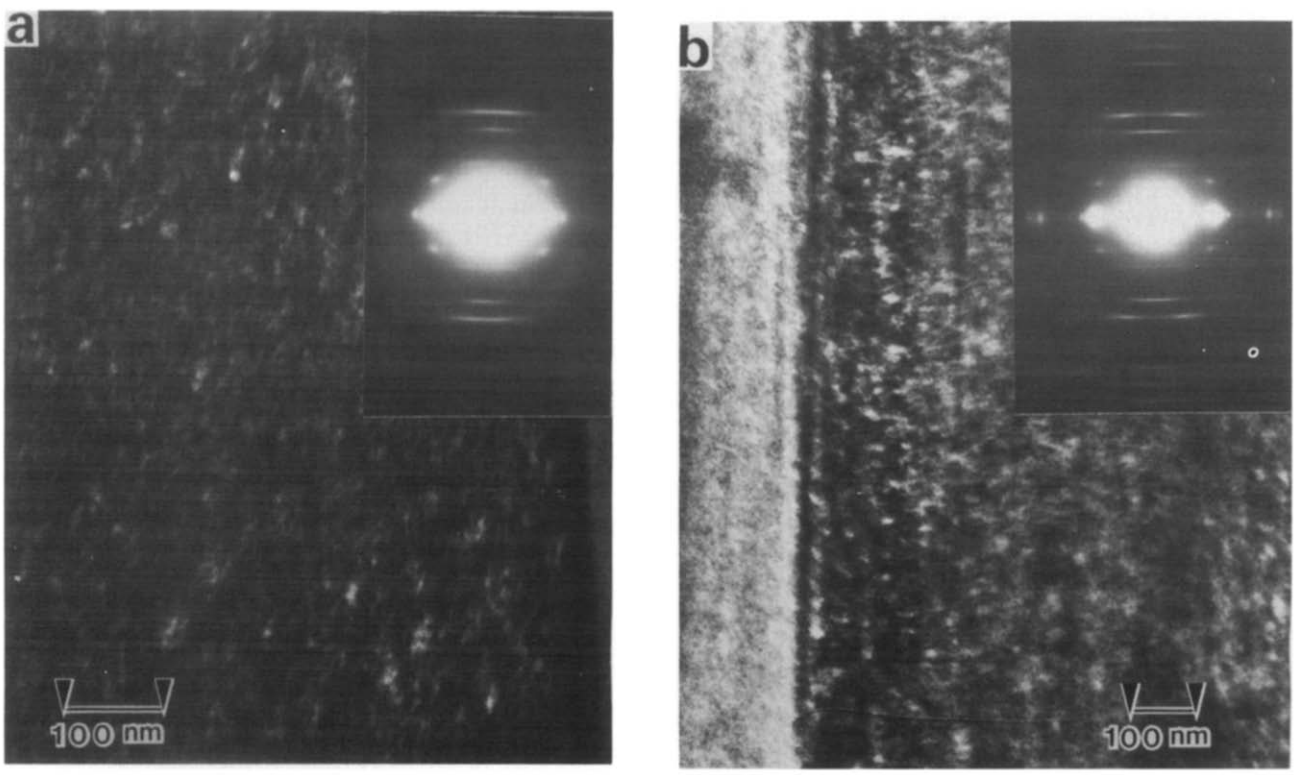

Figure 9 TEM dark field images of PBO fibre in (a) the as-spun and (b) the heat treated condition

tens of nanometres to a few micrometres. ABPBO does not fibrillate as readily as PBO into smaller (≈ 100 nm) fibrils.

Dark field imaging. Dark field TEM images and SAED patterns of as-spun and heat-treated PBO fibre are shown in *Figure 9*. Average crystallite dimensions were determined by measuring the sizes of 10–20 crystallites on a given micrograph. In as-spun fibre they are 5.2 nm (axial)by 5.4 nm (transverse) and grow to 5.7 by 10.6 nm during heat treatment. This results in a decrease in the axial ratio from 0.96 to 0.54. In the as-spun sample, there are occasionally stacks of crystallites three to five high along the fibre axis which are sometimes oriented at an angle to the fibre axis giving a 'chevron' effect. In heat-treated fibre the crystallites in the stacks are virtually all aligned with the fibre axis. The stacking indicates that limited long-range order is present in both the as-spun and the heat treated fibre. Such stacking has not been observed in PBT.

Figure 10 shows dark field images and SAED patterns for as-spun and heat-treated ABPBO fibre. The axial and

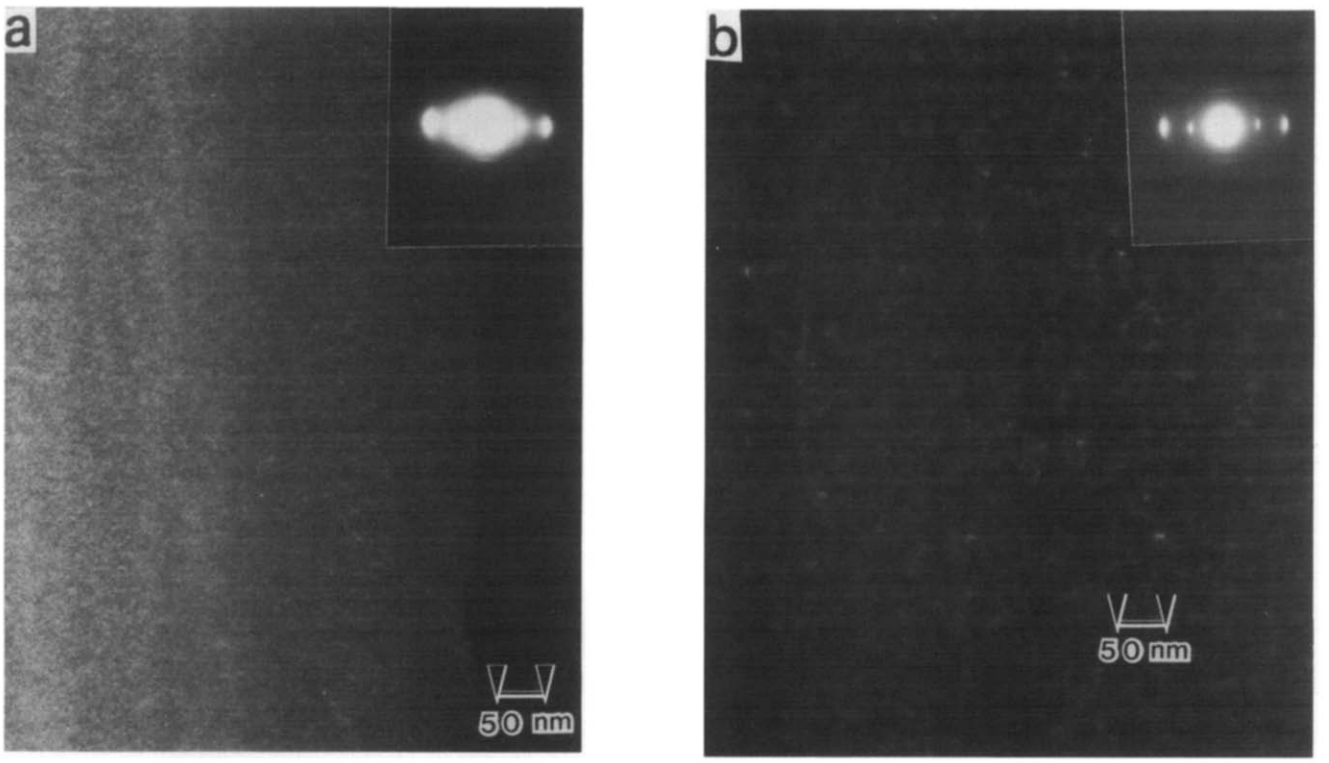

Figure 10 TEM dark field images of ABPBO fibre in (a) the as-spun and (b) the heat treated condition

Table 7 Comparison of crystallite size and axial/transverse ratio of heat treated ordered polymers

Material	Method	Axial size (nm)	Transverse size (nm)	Axial/transverse ratio
PPTA (Kevlar)[4]	WAXS	17.7	6.5	2.7
	TEM BF	15.0	10.0	1.5
PBA (PRD 49)[4]	WAXS	18.4	8.5	2.2
	TEM BF	20.0	17.0	1.2
PBT[14]	TEM DF	19.0	9.0	2.1
PBO – heat treated	TEM DF	5.7	10.6	0.54
ABPBO – heat treated	TEM DF	4.0	5.4	0.74

transverse dimensions increase from about 2.5 by 2.5 nm to 4.0 by 5.4 nm upon heat treatment. Any dimensions reported here below 3 nm should be interpreted cautiously since statistical effects may dominate features in the image[27]. The axial ratio of crystallite dimensions decreases from 1.0 to 0.74 upon heat treatment.

The transverse crystallite sizes of PBO and ABPBO, as measured by dark field imaging, are in reasonable agreement with the values measured in WAXS. Because the dark field (DF) images were taken by isolating the first three equatorial reflections ($E_1+E_2+E_3$) with the objective aperture, it is expected that the mean value measured in DF should lie between the three values for E_1, E_2 and E_3 in WAXS. It is not easy to determine what the most likely value should be for DF imaging for a number of reasons, including texturing effects that change the relative intensities for E_1, E_2 and E_3 (Reference 14), and the effect of size distribution on the WAXS overall breadth.

The results of PBO and ABPBO crystallite size and shape measurements are quite interesting when compared with other ordered polymer systems of PBT, PPTA and poly-*p*-benzamide (PBA – Du Pont's PRD 49). A comparison of typical values of crystallite sizes and axial ratios for heat-treated fibre of PPTA (Kevlar) and PBA, PBT, PBO and ABPBO is presented in *Table 7*. The transverse dimensions of PBO crystallites are generally equal to, or greater than, those of other materials, while the axial dimensions are less than those of other materials by a factor of one half to one eighth. This shape difference is clearly illustrated by the axial ratio, which is 0.54 for PBO and 0.74 for ABPBO, compared to the range of 1.2–2.7 for other ordered polymer systems. This means that PBO crystallites in the heat treated condition are laterally broadened with respect to the fibre axis by a factor of about 2, whereas other ordered polymers are axially elongated by a factor of roughly 2. Crystallites of ABPBO also broaden laterally upon heat treatment, although not to the same extent as PBO.

The reasons for the lateral broadening of PBO or ABPBO crystallites are unclear. While the width of PBO crystallites is similar to other ordered polymers, the axial length is significantly less. Curiously, the length of a 'stack' of three to five crystallites (as found occasionally in

TEM DF of PBO fibre) is 12–20 nm, which is similar to the axial length of crystallites in other ordered polymers. The non-diffracting material between the laterally broadened diffracting regions may be disordered or may be slightly out of the diffraction condition due to a small amount of tilt or twist. One possible explanation is that a stack of laterally broadened crystallites is actually the axial length of a single, larger PBO crystallite. It also seems unusual that rigid-rod polymers, such as PBT and PBO, have crystallites which are 5–20 nm in size along the chain axis while the length of the rigid-rod molecules is 100–200 nm. Thus an unresolved issue in the morphology of rigid-rod and other ordered polymers is, to what extent crystallite size and shape, as measured by TEM DF imaging, are controlled by the factor of polymer morphology and by the factor of TEM imaging conditions. High resolution TEM lattice imaging of ordered polymers may help resolve this issue.

Selected area electron diffraction. The appearance of SAED patterns of PBO and ABPBO fibres was similar to WAXS patterns, although relative intensities and crystallite orientation varied from place to place along a fibril in SAED. The differences in results between TEM SAED patterns and WAXS patterns are a manifestation of a skin-core effect. This is because SAED samples only a very small volume of surface morphology of a TEM sample of a single fibre whereas WAXS averages a much larger volume of the 'bulk' morphology of many whole fibres.

There is strong evidence for the presence of texturing effects (preferred orientation) in PBO and ABPBO, which occurs when small volumes of material are examined in TEM by SAED. The ratio of the intensity of the E_1 reflection to that of the E_2 reflection is not constant. This effect can be explained by the twisting of an individual fibril, which may have a single crystal texture. Twisting of a fibril, as observed in low magnification TEM bright field (BF) imaging, would then cause a variation of the relative intensities of the E_1 and E_2 reflections in SAED. The varying intensities of the E_1 and E_2 reflections for many fibrils examined indicate that texturing exists on an extended scale and may affect fibre mechanical properties. Furthermore, texturing effects could, at least partially, account for differences in SAED and WAXS results with respect to such morphological features as crystallite size and orientation.

GENERAL DISCUSSION

The correlation of structure and morphology to properties of PPTA (Kevlar 49) was first discussed by Northolt[6] and Dobb *et al.*[5] and more recently by Morgan *et al.*[8], Panar *et al.*[10] and Ii *et al.*[28]. The 'bulk' tensile fibre modulus of Kevlar 49, as measured by mechanical testing, is about 110 GPa[6,28,29], while the lattice modulus, as determined by WAXS, has been measured at 168 GPa by Ii *et al.*[28], 182 GPa by Slutsker *et al.*[29] and 200 GPa by Gaymans *et al.*[30]. The lower value of 'bulk' fibre modulus compared with the lattice modulus suggested that a series mechanical model for modulus, with elements of harder crystalline regions and softer disordered regions, would explain the difference in bulk and lattice fibre modulus. In this case, the model of a 'periodically disordered lattice' by Panar *et al.*[10] would be most appropriate. However, an improved PPTA, Kevlar 149, has recently appeared on the market with a modulus of 179 GPa, which approaches the modulus of 200 GPa predicted theoretically by Fielding-Russell[31] and of 232 GPa predicted by Slutsker *et al.*[29]. This means that the 'bulk' fibre modulus is 80–90% of the theoretically predicted value.

The physical basis for achieving a high percentage of the theoretical modulus is not clear, but it may have been attained by 'straightening' the slightly tilted molecular layers discussed in the 'pleated sheet' model[6] or by reducing the fraction of defects or disordered molecules in disordered regions discussed in the 'periodically disordered lattice' model[8]. Thus the recent reports of high 'bulk' fibre modulus indicate that a more likely mechanical model for representing Kevlar structure may be one of parallel elements composed of one element of 'straightened' molecular sheets and another element of material with some defects, disordering or mis-orientation. The tensile strength of a material is dependent on surface flaws for a brittle material or internal defects, e.g. dislocations, for a ductile material. Typically the strength is about 1% of the shear modulus for a ductile material. However, the tensile strength of 2.7–3.4 GPa for PPTA is about 1.5–2% of the theoretical elastic modulus, indicating that the strength in Kevlar is, to some extent, flaw dependent.

Structure-property predictions in PPTA fibre have provided an impetus to improve processing of PPTA fibre to achieve a 'bulk' fibre modulus of 80–90% of the theoretically predicted value. Similar correlations for PBO fibre will now be considered. The 'bulk' fibre tensile modulus of PBT is 320 GPa and of PBO fibres is 370 GPa, while the theoretical modulus of PBT is 600 GPa and of PBO is 615 GPa[32]. The WAXS lattice modulus of PBT fibre has been measured to be 400 GPa and should be similar for PBO fibre, since the structure is similar. Thus, while the 'bulk' modulus of PBO fibre is about 90% of the lattice modulus, it would only be 60% of the theoretical modulus. If a mechanical model with parallel elements is assumed to predict the modulus from the structure, the small difference in 'bulk' and lattice moduli could be accounted for by a small element of material with defects, misoriented material, or disordered material.

The larger difference between the 'bulk' and theoretically predicted modulus must take other factors into account. One factor would certainly be misorientation of molecules from the fibre axis. A model by Northolt and van Aartsen[7] predicts that an average of 3° of chain misorientation (giving an orientation factor, $f_x = -0.495$) would reduce the theoretical modulus by a factor of two. Thus, a marked improvement of the modulus could be achieved by increasing orientation to a value higher than $f_x = -0.489$, which was measured for PBO fibre. The short and long range crystalline order in PBO is much less than in PPTA and an improvement in these factors could also increase modulus. If it were possible to improve processing of PBO fibre to achieve mechanical properties at the same percentage of the theoretically predicted values as those obtained for PPTA fibre, Kevlar 149, this would result in a tensile modulus of 490 GPa and a tensile strength of 10 GPa. These values for PBO fibre are almost triple those of the most recently produced commercial PPTA fibre, Kevlar 149. It will be interesting to see to what extent these values might be

achieved by future improvements in orientation and ordering of PBO fibre through improvements in synthesis and processing.

SUMMARY AND CONCLUSIONS

PBO fibres are composed of fibrillar bundles about 5 μm in diameter and of fine round or ribbon-like fibrils about 0.2 μm in size. The diameter of the bundles and fibrils decreases as a result of heat treatment. Crystallites in as-spun fibre (5.2 nm axial by 5.4 nm transverse) grow during heat treatment to transversely broadened crystallites (5.7 nm axial by 10.6 nm transverse). Crystallites are 3D ordered and also show limited long-range order in TEM by stacking three to five high, sometimes oriented at an oblique angle to the fibre axis in the as-spun fibre. Molecules and crystallites are highly oriented in both as-spun and heat treated fibre. Crystallographic texturing and a skin-core effect were observed on a scale of 10–100 nm.

ABPBO fibre has fibrillar bundles and fibrils which were coarser and rounder than in PBO fibres. Crystallites in as-spun fibre (2.5 nm axial by 2.5 nm transverse) grew during heat treatment to transversely broadened crystallites (4.0 nm axial by 5.4 nm transverse), while 3D crystalline order also increased. Fibre orientation increased and *c*-axis paracrystalline disorder decreased significantly as a result of tension heat treatment, probably due to increased conformational ordering by chain extension. ABPBO fibres also showed texturing and skin-core effects.

PBO and ABPBO fibres differ from PBT fibre in that they have greater 3D crystalline order, transversely broadened crystallite shape, and limited long-range order in the form of crystallite stacking. However PPTA fibre has greater 3D crystalline order and also greater long range order with 200–500 nm axially oriented, hydrogen-bonded pleated sheets.

Improvements in the orientation and ordering of PBO fibre through improvements in the synthesis and processing of PBO may, based upon theoretically predicted values, result in mechanical properties of 490 GPa tensile modulus and 10 GPa tensile strength, almost triple that of the most recently produced commercial PPTA fibre, Kevlar 149.

REFERENCES

1 Wolfe, J. F., Loo, B. H. and Arnold, F. E. *Polym. Prepr. Am. Chem. Soc. Div. Polym. Chem.* 1978, **19**, 1
2 Wolfe, J. F., Sybert P. D. and Sybert, J. R. US Patent 4 533 693, 1985
3 Bennett, S. C., Dobb, M. G., Johnson, D. J., Murray, R. and Saville, B. P. 'Electron Microscopy Analysis Group Conference Proceedings', Academic Press, New York, 1975, p. 329
4 Dobb, M. G., Johnson, D. J. and Saville, B. P. *J. Polym. Sci. Polym. Symp.* 1977, **58**, 237
5 Dobb, M. G., Johnson, D. J. and Saville, B. P. *J. Polym. Sci. Polym. Phys. Edn* 1977, **15**, 2201
6 Northolt, M. G. *Eng. Polym. J.* 1974, **10**, 799
7 Northolt, M. G. and Van Aartsen, J. *J. Polym. Sci. Polym. Symp.* 1977, **58**, 283
8 Morgan, R. J., Pruneda, C. O. and Steele, W. J. *J. Polym. Sci., Polym. Phys. Edn* 1983, **21**, 1757
9 Li, L. S., Allard, L. F. and Bigelow, W. C. *J. Macromol. Sci., Phys. Edn* 1983, **B22**, 269
10 Panar, M., Avakian, P., Blume, R. C., Gardner, K. H., Gierke, T. D. and Yang, H. H. *J. Polym. Sci., Polym. Phys. Edn* 1983, **21**, 1955
11 Sawyer, L. *J. Polym. Sci. Polymer Lett.* 1984, **22**, 347
12 Chanzy, H. D., Smith, P., Revol, J.-F. and St John Manley, R. *Polym. Commun.* 1987, **28**, 133
13 Thomas, E. L., Farris, R. J., Hsu, S. L., Allen, S., Filippov, A., Minter, J., Roche, E., Shimamura, K., Takahashi, T. and Venkatesh, G. US Air Force Technical Report AFWAL-TR-80-4045, vol. III, Part I, 1982
14 Minter, J. R. *Ph.D. Dissertation*, University of Massachusetts, 1982
15 Minter, J. R., Shimamura, K. and Thomas, E. L. *J. Mater. Sci.* 1981, **16**, 3303
16 Shimamura, K., Minter, J. R. and Thomas, E. L. *J. Mater. Sci. Lett.* 1983, **2**, 54
17 Odell, J. A., Keller, A., Atkins, E. D. T. and Miles, M. J. *J. Mater. Sci.* 1981, **16**, 3039
18 Wellman, M. W., Adams, W. W., Wiff, D. R. and Fratini, A. V. US Air Force Technical Report AFWAL-TR-79-4184, 1980
19 Fratini, A. V. and Adams, W. W. *Am. Crystallogr. Assoc. Abstr.* 1985, **13**, 72
20 Fratini, A. V., Cross, E. M., O'Brien, J. F. and Adams, W. W. *J. Macromol. Sci., Phys. Edn* 1985–1986, **B24**, 159
21 Krause, S. J. and Adams, W. W. *Proc. Electron Microsc. Soc. Am.* 1984, **42**, 382
22 Fratini, A. V. personal communication
23 Hosemann, R. and Wilke, W. *Die Makromol. Chem.* 1968, **188**, 230
24 Kumar, S., Krause, S. J. and Adams, W. W. *Proc. Electron Microsc. Soc. Am.* 1985, **43**, 84
25 Adams, W. W. unpublished results
26 Hwang, W-F., Wiff, D. R., Benner, C. L. and Helminiak, T. E. *J. Macromol. Sci. Phys.* 1983, **B22**, 231
27 Roche, E. J. and Thomas, E. L. *Polymer* 1981, **22**, 333
28 Ii, T., Tashiro, K., Kobayashi, M. and Tadokoro, H. *Macromolecules* 1987, **20**, 347
29 Slutsker, L. I., Utevskii, L. E., Chereiskii, Z., Yu, Z. and Perepelkin, K. E. *J. Polym. Sci. Polym. Symp.* 1977, **58**, 339
30 Gaymans, R. G., Tijssen, J., Harkama, S. and Bantjes, A. *Polymer* 1976, **17**, 517
31 Fielding-Russell, G. S. *Text. Res. J.* 1971, **41**, 860
32 Adams, W. W., Lenhert, P. G., Stewart, J. P., Klei, H. E., Eby, R. K., Jiang, H. and Smith, J. *Bull. Am. Phys. Soc.* 1987, **32**, 780